An Electronic Structure Study: The Case of $YbRh_2Si_2$

G.A. Wigger, F. Baumberger, and Z.-X. Shen
Department of Applied Physics and Stanford Synchrotron Radiation Laboratory, Stanford University, Stanford, California 94305

Z. P. Yin, W.E. Pickett, S. Maquilon, and Z. Fisk
Department of Physics, University of California, Davis, California 95616
(Dated: September 11, 2006)

The electronic properties of $YbRh_2Si_2$ are studied by an ab initio band structure calculation in a relativistic framework including correlation corrections and angle-resolved photoemission experiments. The calculated band structure manifests a 4^{13} spin-polarized configuration leaving the $m = 0$ $4f$ state unoccupied at 1.4 eV above the Fermi energy. Contrary to previous results, the $4f$ bands are located far below the Fermi level and the anisotropic Coulomb interaction within the $4f$ shell splits the multilevel into broader $4f$ complexes. The first photoemission spectra obtained on $YbRh_2Si_2$ show an obvious f-multilevel splitting into $j = 7/2$ and $5/2$ excitations. An analysis according Anderson's single impurity model, explains the photoemission spectra in accordance with the results of the band structure calculations and various macroscopic experiments. The strong hybridization shifts the spectral weight of the $4f_{7/2}$-level close to the Fermi energy where it hybridizes with the Rh-d bands. The recent mixed-valency of $YbRh_2Si_2$ is rejected from both theory and experiment. We discuss our findings with respect to two rivaling theories for quantum criticality, i.e. spin-density-waves versus composite quasiparticles.

PACS numbers: Valid PACS appear here

I. INTRODUCTION

Heavy fermions (HF) on the border to a zero-temperature magnetic transition have been particularly attractive in the past years [1] because of their anomalous low-temperature thermodynamic, transport and magnetic properties that deviate strongly from Landau Fermi Liquid (LFL) theory. Recently, an increasing number of examples of Ce and U based systems such as $CeCu_{6-x}Au_x$, $CePd_2Si_2$, $CeIn_3$ and U_2Pt_2In have been found to exhibit magnetic quantum criticality by either doping- or pressure-tuning.[2–5] $YbRh_2Si_2$ has attracted attention as the first observed Yb-based and stoichiometric HF system with competing Kondo and Ruderman-Kittel-Kasuya-Yosida (RKKY) interaction, the dominant exchange mechanisms in metals where the moments interact through the intermediary conduction electrons [6]. Pronounced non-Fermi Liquid (NFL) behavior has been observed in the resistivity $\rho(T)$ and the electronic specific heat $\Delta C(T)$ at low temperatures showing $\Delta\rho = \rho - \rho_0 \propto T$ and $\Delta C/T \propto$ - $ln(T)$, respectively.[7, 8] The ground state properties of $YbRh_2Si_2$ can be easily tuned around the magnetic quantum critical point (QCP) by control parameters such as pressure, magnetic field or doping.[1] An external pressure compresses the atomic lattice leading to an increase of the antiferromagnetic coupling with a maximal Néel temperature of 1 K at 2.7 GPa.[7, 9] On the other hand, expanding the lattice by replacing Si by Ge [10] or Yb by La favors the Kondo coupling and reduces T_N. Approximately 5 % Ge- or La-doping completely destroys the antiferromagnetic order in $YbRh_2Si_2$. Electron spin resonance (ESR) and nuclear magnetic resonance (NMR) experiments have demonstrated the importance of magnetic fluctuations at low T.[11, 12] A Hall effect measurement suggests a discontinuity in the FS volume of 1 charge carrier across the quantum phase transition.[13] Based on a local density approximation (LDA) calculation, the change in the FS volume by 1 charge was suggested to arise from a shift of the f-levels across a quantum transition from the antiferromagnetic phase to the Kondo Fermi liquid.[14] At intermediate temperatures, a regime establishes itself where the quantum critical fluctuations dominate, and for which it is believed that the notion of a well defined quasiparticle breaks down. Remarkably, in $YbRh_2Si_2$ this regime extends up to 10 K.[8]

We distinguish various theories about antiferromagnetic metallic Kondo lattices. In the weak coupling limit, the magnetism is viewed as a spin-density wave (SDW) instability that develops out of the parent heavy Fermi-liquid state and a small magnetic moment is observed. Using Gaussian critical fluctuations, Hertz,[15] and in a refined version Millis,[16] have given the first phase diagrams for the weak-coupling limit. The internal structure of the quasiparticle is unimportant and the interaction between the Fermi surface and the critical antiferromagnetic spin fluctuation dominate at low temperatures. Indeed, in $YbRh_2Si_2$, a very weak antiferromagnetic (AFM) order with a tiny magnetic moment of $\mu_{Yb} \approx (10^{-2} - 10^{-3})\mu_B$ [11] is observed at ambient pressure below the Néel temperature $T_N \simeq 70$ mK. This initially favored the idea that $YbRh_2Si_2$ belongs to the class of SDW metals close to the magnetic QCP, but severe conflicts with several experiments rouse doubts. In the strong-coupling limit, the localized f-states, giving rise to a large high-temperature magnetic moment, couple through the Kondo effect to itinerant states. This induces a Fermi surface of heavy composite quasiparticles.

Recently, a detailed phase diagram on heavy fermions in this strong-coupling limit was given by Senthil and collaborators.[17, 18] The ground states at the QCP is described by an exotic phase where the heavy quasiparticles decay into a magnetic (neutral spinon) and an electronic (spinless fermion) excitation. This effect is called the fractionalization of the FS, i.e. the fragmentation of the FS into a 'cold' and a 'hot' sheet.[17, 19] The latter consists of heavy quasiparticles derived from electronic states with f-symmetry. More recently, Si and coworkers introduced a local quantum critical point (LQC), named so because long wavelength and spatially local critical modes coexist at this point.[20, 21] Again, for material close to LQC points, a large magnetic moment at high temperatures is allowed which is then progressively screened by the Kondo effect at low temperatures. In either the SDW or the LQC case, the f-electrons are expected to be partly integrated into a large Fermi surface (FS), however for the latter the quasiparticle residue Z vanishes at the QCP and hence no Kondo resonance is expected to appear in the photoemission spectrum.[21]

A direct measurement of the electronic band structure and especially the location and renormalization of f-derived electronic bands, their hybridization with the conduction bands and their incorporation into the FS could provide a stringent test of such theories. Angle-resolved photoemission spectroscopy (ARPES) has proven to be uniquely powerful in its capability to directly probe the electronic structure of solids.[22]

In this article, we report sophisticated band structure calculations in agreement with the first ARPES experiments for $YbRh_2Si_2$ in the ordinary high-temperature FL state where the quasiparticles are expected to be well defined. We perform an analysis of the $4f$-derived spectrum $\rho_\nu(\epsilon)$ within the single-impurity Anderson model (SIAM).[23] This analysis explains $\rho_\nu(\epsilon)$ using the results from the band structure calculation perfectly in agreement with the results from macroscopic experiments. The hybridization of the electronic f-levels with two valence bands shifts the spectral weight close to E_F and opens electronic gaps of 91 and 45 meV, respectively. The electronic configuration of the Yb-ion is nearly $4f^{13}$ and the strong Kondo coupling regime is established. The occurrence of Yb in a mixed-valent state in this compound is hence experimentally rejected and of fundamental importance to develop a comprehensive understanding of the low-temperature behavior of $YbRh_2Si_2$.

II. ELECTRONIC STRUCTURE CALCULATIONS

A. Structure

The crystal structure of $YbRh_2Si_2$, displayed in Fig. 1, is bct with $I4/mmm$ space group (No. 139). The Yb ion occupies the $2a$ site which has full tetragonal $4/mmm$ symmetry and forms a bct sublattice, which becomes important in the interpretation of its magnetic behavior. Rh resides in a $4d$ site ($\bar{4}m2$ symmetry), and lie on a simple tetragonal sublattice rotated by 45° in the plane and having lattice constants $a/\sqrt{2}$ and $c/2$. Si is in the 4e site ($4mm$); the Si-Si interatomic distances 2.46 Å is only 5% longer than in diamond structure Si, so one view of the structure is in terms of Si_2 dimers oriented along the $\hat{z}$ axis. Yb atoms and the dimers form a centered square lattice in the $x-y$ plane. Yb is eightfold coordinated by Rh at a distance of 3.17 Å. The atomic positions are [in units of (a,a,c)]: Yb (0,0,0), Rh $(0,\frac{1}{2},\frac{1}{4})$, Si (0,0,0.375); note that the Si height is not determined by symmetry and is accidentally equal to $\frac{3}{8}$. The experimental lattice constants $a = 4.010$ Å and $c = 9.841$ Å have been used in our calculations.

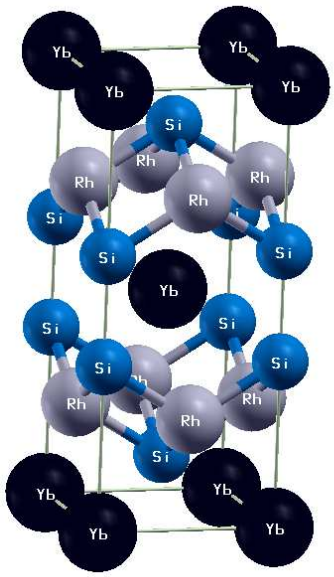

FIG. 1: (Color online) Crystal structure of $YbRh_2Si_2$.

B. Methods

Rare earth atoms, and other atoms with strong effective intraatomic Coulomb repulsion U (Hubbard U) pose a serious challenge for band theoretical methods. Density functional theory addresses at the most basic level the ground state, which gives the Hund's rule ground state of the Yb ion a central role. Hund's rule implies that one leaves consideration of spin-orbit coupling (SOC) until after the spin S and angular momentum L have been maximized. For interpreting single-particle-like excitations, which is the main topic of this paper, one wants to obtain the $j = \ell \pm \frac{1}{2}$ character of the excitations (which is evident in spectra). Thus one must include SOC at the one-electron level, and that is the viewpoint that we

take here. From the Curie-Weiss susceptibility at high temperature in $YbRh_2Si_2$ it is clear that the Yb ion is primarily in an $4f^{13}$ configuration (at elevated temperature, at least), corresponding to $S = \frac{1}{2}$, $L = 3$, $J = \frac{7}{2}$ in the absence of crystal fields.

To be able to include the necessary combination of exchange splitting (magnetic order), SOC, and also the LDA+U approach that is necessary for rare earth atoms, we have used the Wien2k electronic structure code.[24] With magnetization along (001) direction, spin-orbit coupling reduces the symmetry to $Abm2$ (#39). The around-mean-field version of LDA+U was used, with $U_{eff} = U - J = 7.0$ eV. Only the m=0 $4f$ orbital was unoccupied. We use a k mesh of 20^3 (641 k-points in the IBZ), $R\,K_{max}$=9, and the Perdew-Burke-Ernzerhof generalized gradient approximation[25] for exchange correlation potential. An energy range from -7.00 Ry to 7.00 Ry is used when SOC is incorporated.

C. Band Structure Results

The band structure shown in Fig. 2 is characterized by the expected $4f^{13}$ spin-polarized configuration of the Yb ion. Without SOC this would correspond to one hole in the minority $4f$ shell. With SOC included, as here, the flat $4f$ band complex is spin-mixed and split into a $4f_{5/2}$ complex and a $4f_{7/2}$ complex separated by the spin-orbit splitting of roughly 1.3 eV. Although each $4f$ band is quite flat, each of these complexes of $2j+1$ bands ($j = \frac{5}{2}, \frac{7}{2}$) is split somewhat due to the anisotropy of the Coulomb interaction[26] within the $4f$ shell, which is included fully in the LDA+U method. However, the $4f$ electrons are polarized (one hole, S=$\frac{1}{2}$) so there is also an exchange splitting which complicates the identification in the figure of the $4f_{5/2}$ and $4f_{7/2}$ states separtely. However, the result that is pertinent to this paper is that this electronic structure calculation fully includes magnetic and relativistic effects, and leaves one hole in the $4f$ shell consistent with the Curie-Weiss susceptibility.

The unoccupied $4f$ band lies 1.4 eV above the Fermi level E_F and can be seen to mix exceedingly weakly with the itinerant (Rh+Yb+Si) bands The occupied levels lie 3.4 eV or more below E_F and also hybridize weakly. Hence at the band structure level the $4f$ states are well away from the Fermi level. We focus first on the states near and at E_F, and then return to the (Kondo) coupling of the $4f$ moment to the Fermi surfaces.

The total Rh $4d$ and total Yb $5d$ character are shown separately in the fatband representations in Fig. 2. Much of the Rh $4d$ bands are occupied, while most of the Yb $5d$ bands are unoccupied, however there is Yb $5d$ character around and below the Fermi level. The Si $2p$ character is spread fairly evenly through the valence and conduction bands. The bands around E_F have mostly Rh $4d$ character, with some Yb $5d$ mixed in, and the bands along symmetry lines are clearly associated with certain symmetry-determined irreducible representations a_g

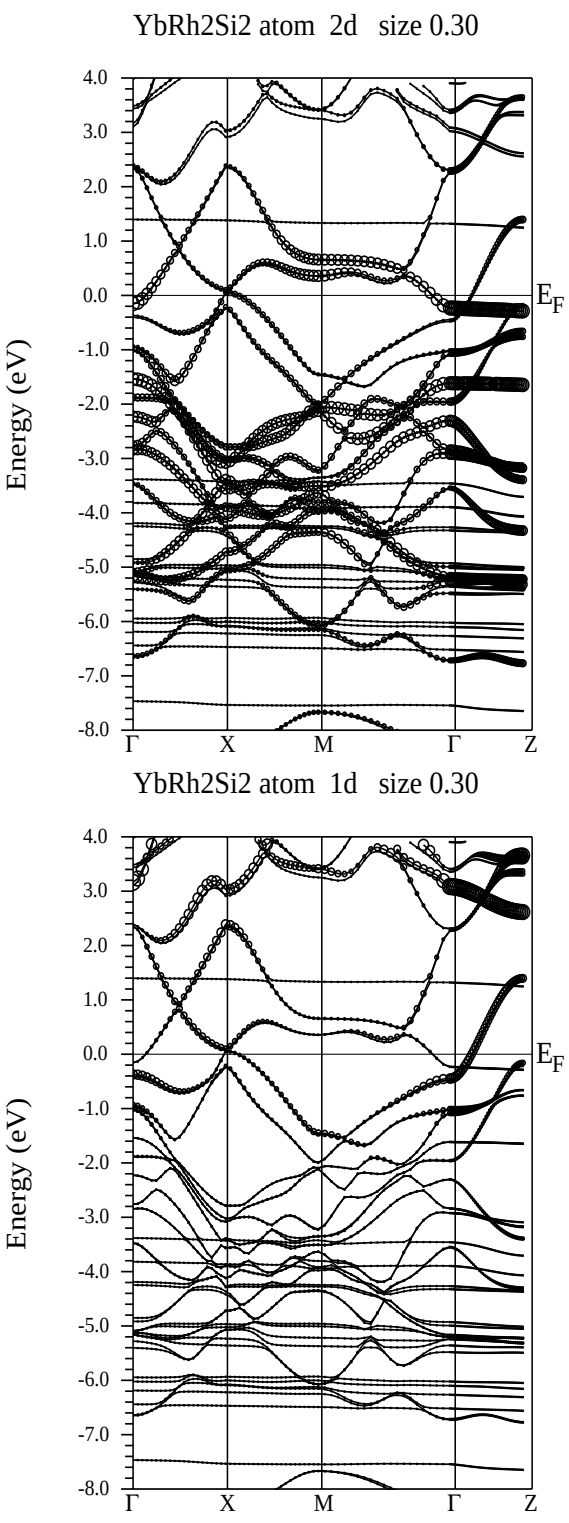

FIG. 2: Band structure of $YbRh_2Si_2$ along tetragonal symmetry lines. The Cartesian symmetry line indices are Γ(0,0,0), X(1,0,0), M(1,1,0.0), Z(0,0,1), in units of $[\frac{\pi}{a}, \frac{\pi}{a}, \frac{2\pi}{c}]$. Top panel: bands with total Rh $4d$ emphasized using the fatbands representation. Bottom panel: same bands with total Yb $5d$ emphasized using the fatbands representation.

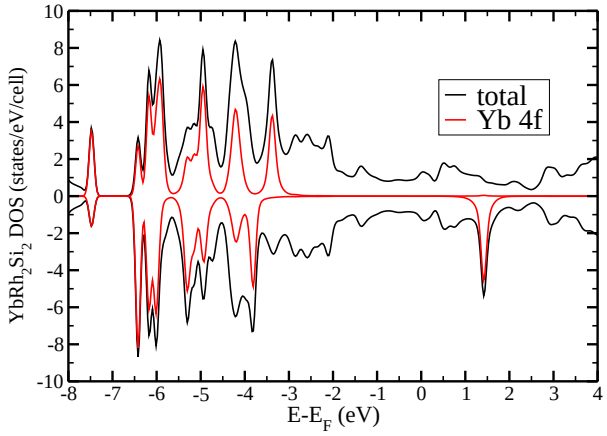

FIG. 3: (Color online) Total, and Yb $4f$ projected, density of states of $YbRh_2Si_2$ corresponding to the band structure in Fig. 2.

$(d_{3z^2-r^2})$, $b_{1g}(d_{x^2-y^2}), b_{2g}(d_{xy})$ or $e_g(d_{xz}, d_{yz})$ of the Rh and Yb d states.

The first noteworthy feature is the band lying 0.1 eV below E_F at Γ, which is completely flat along $\Gamma - Z$ and disperses upward in the plane: this is a pure Rh $d_{x^2-y^2}$ band, whose two-dimensionality near the band edge will give rise to a (small) step increase in the density of states N(E). There is also strong Rh $4d_{x^2-y^2}$ character at -5 eV (within the $4f$ bands), presumably the bonding combination of the two Rh atoms in the cell. The Rh $d_{x^2-y^2}$ band crossing E_F contributes the cylindrical faces of the electron-type tall pillbox $\mathcal{P}$ Fermi surface (FS) with (near circular) mean radius in the plane of k_F=0.133 $\frac{\pi}{a}$. All three FSs are displayed in Fig. 4. The Fermi level is intersected along $\Gamma - Z$ by a band composed of Rh $4d_{3z^2-r^2}$, Yb $5d_{3z^2-r^2}$ character and 2 eV wide. This band defines the top and bottom faces of the Γ-centered pillbox, with Fermi wavevector $k_F = 0.265\frac{2\pi}{c}$ along the $\hat{z}$ axis.

From the bands in Fig. 2 it can be observed that a hole-type surface nearly closes at the X=$(\frac{\pi}{a}, 0, 0)$ point. Because the point we call X is not on the bct Brillouin zone boundary (the true zone is shown in Fig. 4), this is not a small ellipsoid as might be guessed, but rather part of tubes of a multiply connected jungle gym surface $\mathcal{J}$. The largest part of this surface encircles nearly all of the upper zone face centered on the Z=$(0, 0, \frac{2\pi}{c})$ point. The character near X is Rh $4d_{xz}, 4d_{yz}$, and some Yb $5d$ character. There is also strong Rh $4d_{xz}, 4d_{yz}$ character in the flat band along $\Gamma - Z$ near -3 eV. Rh $4d_{xy}$ character dominates the flat band at -1.5 eV along $\Gamma - Z$, which disperses downward from there within the plane.

$YbRh_2Si_2$ is a heavy fermion compound, whose $J = L + S = \frac{7}{2}$ ion and associated local moment will be affected by crystal fields and finally screened by conduction electrons at low temperature (a tiny moment survives and orders in $YbRh_2Si_2$). Thus, while our ferromagnetic state with $S = \frac{1}{2}$ is not expected to describe the interacting ground state, it has the virtue of providing the degree of Kondo coupling of the Yb moment to the two Fermi surfaces. The exchange splitting of the Γ spheroid is 6 meV around its waist (in the $x - y$ plane) and 30 meV at top and bottom. For the hole pancake, the splitting is 19-20 meV along all axes.

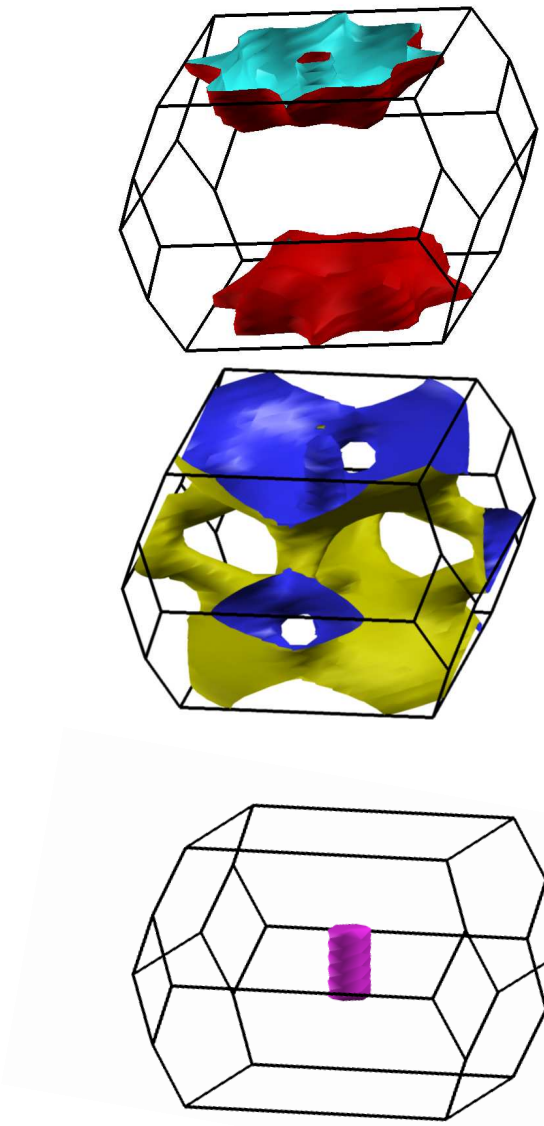

FIG. 4: The three Fermi surfaces of $YbRh_2Si_2$ with $4f^{13}$ configuration, pictured within the crystallographic Brillouin zone. Top panel: fluted donut $\mathcal{D}$ surface centered around the upper zone face midpoint Z. Middle panel: multiply-connected jungle gym $\mathcal{J}$ surface, ... Bottom panel: tall pillbox surface $\mathcal{P}$, containing electrons at the zone center Γ.

D. Discussion of Bands and Fermi Surfaces

This fully relativistic, spin-polarized LDA+U band structure and resulting Fermi surfaces can be compared with those of Norman,[14] who presented unpolarized relativistic LDA predictions. Not surprisingly there are substantial differences, as expected from Norman's $4d^{14}$ configuration versus our magnetic $4f^{13}$ bands; this difference in Yb $4f$ charge state puts Norman's Fermi level one electron lower with respect to the Rh $4d$ + Yb $5d$ + Si $2p$ itinerant bands. As the result, the flat Rh $4d_{x^2-y^2}$ band that lies 0.1 eV below E_F in our bands lies 0.1 eV *above* E_F in the LDA bands, and the Fermi surfaces are entirely different. This will lead to a different prediction for the Hall coefficient.

However, on the qualitative level, our Fermi surfaces include large sheets with canceling positive and negative contributions to the Hall coefficient, as do Norman's. The Hall coefficient, being a FS average of the inverse curvature, will bear no relation to the number of carriers. Discussion of the Hall tensor will be deferred to a future publication. No doubt it will be quite anisotropic, given the strong tetragonality of the FSs. The edges of the pillbox P may give large contributions (and make evaluation difficult); likewise, the sharp edges on the donut D will also have large curvatures.

III. EXPERIMENTS

Single crystalline platelets of $YbRh_2Si_2$ were grown by the flux-growth method using an In flux in a sealed Ta tube under argon atmosphere. The crystals were washed in HCl acid solution to safely remove excess In flux. The tetragonal crystal structure and the lattice parameters were confirmed by X-ray powder diffraction.

The ARPES measurements were performed using a chamber equipped with a Scienta SES200 analyzer attached to the undulator beamline 5-4 of Stanford Synchrotron Radiation Laboratory (SSRL) and a second vacuum system equipped with a Scienta SES2002 analyzer and a microwave driven monochromatized He-discharge lamp (Gammadata VUV5000). At SSRL, we used linearly polarized photons of 21.4 eV. We intentionally refrained from tuning the photon energy to resonance with Yb-core levels which enhances the photoelectron yield of the Yb $4f$-electrons but worsens the energy resolution by approximately 6-8 times. An energy resolution of $\sim$ 40 meV or more would hide the relevant hybridization features for the critical system $YbRh_2Si_2$. The total energy resolution including the monochromator and the analyzer was 8 meV for the 21.2 eV beam, and 22 meV for the 21.4 eV beam, respectively. The chamber pressure was below $4{\cdot}10^{-11}$ torr. The samples were cleaved in situ at $T \sim 14$ K. The position of the Fermi level (E_F) was calibrated from the Fermi edge of polycristalline Au for every measurement.

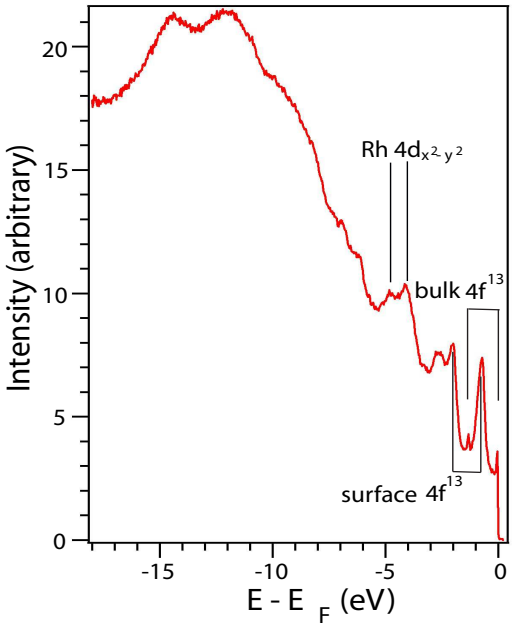

FIG. 5: (Color online) Angle-integrated PE spectrum (red curve) of $YbRh_2Si_2$ measured with photon energy of 40.8 eV at 14 K. The lines are explained in subsection IV A.

IV. PHOTOEMISSION RESULTS AND DISCUSSION

A. angle-integrated spectrum at $h\nu = 40.8$ eV

Fig. 5 shows the angle-integrated spectrum (red curve) for angles between -5° and 17° measured with He-II radiation. The broad distribution of intensity below -8 eV, indicated by the shaded area if Fig. 5, is due to the Si 3s bands, as suggested by the band structure calculations. At low binding energies, we can identify two sharp but small intensity maxima at $\sim$ - 1.3 eV and right at E_F with a peak intensity ratio of approximately 2:3, respectively. The corresponding plot for $h\nu = 21.2$ eV does not display any pronounced intensity at these energies. Hence, these are the bulk $4f^{13}$ peaks, separated by 1.3 eV as suggested by the band structure calculation (see section IV C). The very intense flat bands at 650 meV and at 2 eV can be attributed to the spin-orbit splitted surface bands [27] originating from Yb-ions at or close to the sample surface (The relative intensity of surface vs. bulk peak decreases strongly when the photon energy is increased from 21 to 41 eV and considering Refs. [22, 28, 32]). The intensity around 3 eV is not due to flat bands but is a result of various co-terminating band edges having high intensities in that energy region (see therefore the angle-resolved spectrum in Fig. 6). In the angle-resolved spectrum (not shown here), we observe a very flat band also at -5 eV. Little dispersion is observed in the angle-resolved photoemission spectrum which makes us believe that this peak at -5 eV can be attributed to

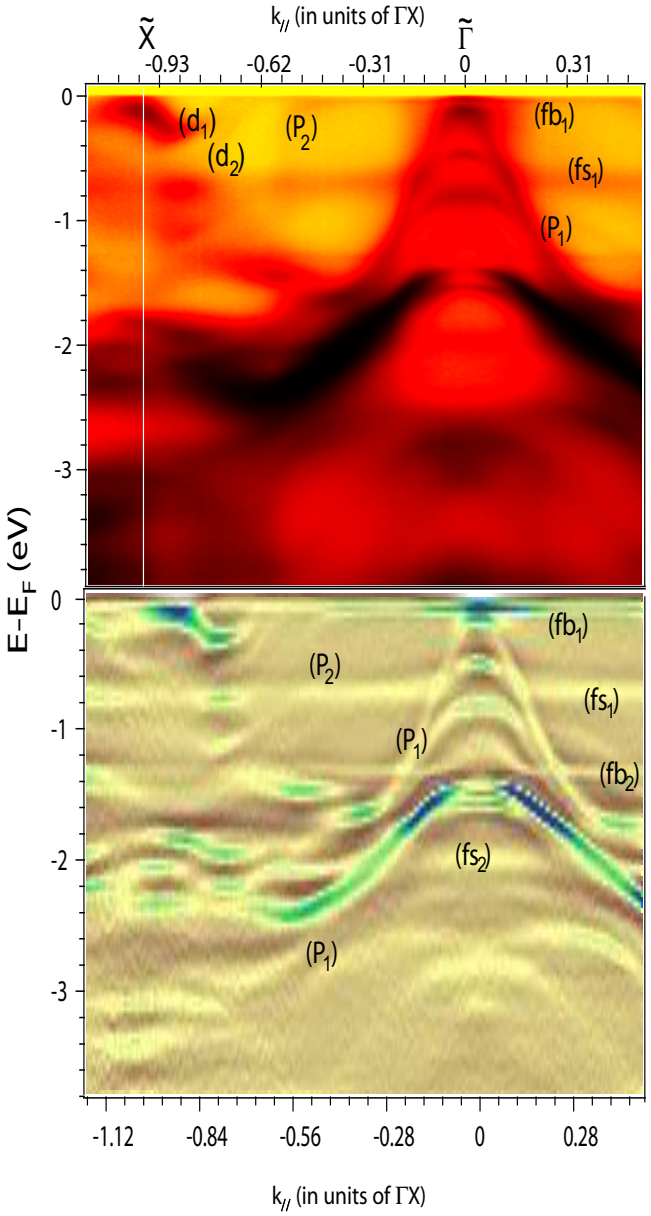

FIG. 6: (Color online) Angle resolved PE spectra taken at $h\nu$ = 21.4 eV at T = 14 K in the Γ-X-Z plane. The lower panel shows the second derivative of the spectrum (upper panel). The relevant bands are denoted as (fb_1) and (fb_2) for the bulk $4f^{13}$ and (fs_1) and (fs_2) for the surface $4f^{13}$ states, P_1 and P_2 are valence bands with mostly Rh-4d- and partly Yb-5d-character for the latter one.

the bonding Rh $4d_{x^2-y^2}$ orbitals.

B. Photoemission spectra for $h\nu$ = 21.4 and 21.2 eV

Within the sudden approximation,[22] angle-resolved photoemission measures the single-particle spectral function $A(\vec{k},\omega)$. In the Landau theory of Fermi liquids, the spectral function is determined by the bare band structure ϵ_k and the complex self energy $\Sigma = \Sigma' + \mathrm{i}\cdot\Sigma''$ as:

$$A(\vec{k},\omega) = \frac{1}{\pi}\frac{\Sigma''(\vec{k},\omega)}{\left[\omega-\epsilon_k-\Sigma'(\vec{k},\omega)\right]^2+\left[\Sigma''(\vec{k},\omega)\right]^2} \quad (1)$$

The upper panel of Fig. 6 shows an angle-resolved photoemission spectrum $A(\vec{k},\omega)$ in the $\Gamma-X-Z$-plane, where $\vec{k}$ is the angular momentum in plane and ω the photohole energy, taken at a beam energy $h\nu$ = 21.4 eV. In order to connect to the calculations, we use ω, ϵ and E-E_F on an equal basis in the following discussions. $\tilde{\Gamma}$ denotes the center (equivalent to Γ), the thin white line indicates the $\tilde{X}$-point. The distance $\tilde{\Gamma}\tilde{X}$ is equivalent to ΓX in the center of the Brillouin zone (BZ). Comparing the EDC and the FS images to the results of the band structure calculations we believe that $\tilde{\Gamma}$ lies approximately at 2/3 of the distance between Γ and Z. Two different flat bands display a pronounced intensity, band (fb_1) located very close to E_F, and band (fs_1) with a maximum intensity at ≈ 680 meV below E_F. The latter derives from electronic states of Yb atoms close to the sample surface (see subsection IV A). Previous spectroscopic experiments [29] and fully relativistic calculations (see Fig. 2) revealed that the spin-orbit interaction in Yb-based materials is considerable. The $4f_{5/2}$-levels usually have 1.0 - 1.5 eV higher binding energies than the $4f_{7/2}$ multiplet, consistent with the 1.3 eV value obtained within the relativistic calculation (see section II). Masked in the primary spectra by the high intensity of neighboring bands, the second derivative plot (lower panel of Fig. 6) reveals a third very flat electronic band (fb_2) separated from band (fb_1) by the spin-orbit splitting $\Delta\epsilon_f \approx 1.3$ eV and a forth flat band (fs_2) 1.3 eV below band (fs_1), i.e. the bulk and surface $4f^{13}_{5/2}$ states, respectively. Neither a careful investigation of the spectra nor the second derivative plot revealed an additional flat band with f-symmetry as indicated by the LDA+U+SOC band structure calculation. This observation strongly favors the notion of $4f$ single particle-like excitations separated into a $4f_{5/2}$-multilevel at binding energies ∼ 1.3 eV and a sharp band of $4f$-electrons with j = 7/2 centered at ∼ 45 meV below E_F and with a line width of $\Gamma_{FWHM} \approx 30$ meV. A strong intensity is displayed by the band (P_1) which shows nearly a free electron parabola with band width B down to -3.6 eV at the X-point. This bulk band is characterized mostly by Rh-4d symmetry (see the flatbands representation in Fig. 2). Keeping in this simplistic nearly-free electron picture, we can make out a continuation of this parabola for $\epsilon > 0$ eV. We will use this bands for the simulation of the $4f$-spectral weight below. Moreover, band (P_1) also distorts the Yb-derived surface band (fs_1) and (fs_2) around $\tilde{\Gamma}$. The colour of the cleaved samples indicates that the Si-atoms along the c-axis forming very strongly bonded dimers build the top-most layer. Hence, the first Yb-layer is intermediate between a bulk and a

surface layer such that it can be distorted by hybridization with a bulk band. The hybridization is clearly reduced and the line width broadened. Half-way between the $\tilde{\Gamma}$ and the $\tilde{\mathrm{X}}$ point, a band (P_2), displaying a very weak intensity, hybridizes with the f-band. We will show in Fig. 7 how this hybridization arises. This band P_2 can be found in Fig. 2, where it starts at 2 eV above E_F at Γ dispersing down and crossing E_F near X, reaching -2 eV close to M. This band induces the hole-like FS D. At $\sim$ 20-25 angular degrees, we observe two different bands denoted as (d_1) and (d_2). They form the jungle gym FS sheet and will be briefly discussed in the subsection IV D.

The upper left panel of Fig. 7 shows the photoemission spectrum $A(\overrightarrow{k},\omega)$ taken in the vicinity of $\tilde{\Gamma}$ using a photon energy of 21.2 eV. At very small angles, the $4f_{7/2}$-band (1) with band width less than 35 meV hybridizes weakly with the Rh $4d$ band leading to a dispersion of $\approx$ 10 meV. A gap between the peaks of the two bands of approximately 80 meV is observed. For $\omega \leq 20$ meV, $A(\overrightarrow{k},\omega)$ rises again towards lower binding energies indicating a double peak structure. A comparison to the band structure calculations suggests that this additional feature originates from the Rh $4d_{x^2-y^2}$ band crossing E_F at $\tilde{\Gamma}$ and hybridizing weakly with the $4f$ band. This effect shifts the spectral weight from the band closer to E_F and flattens it, so nearly no dispersion is observed. We note here, that this feature near E_F does not follow the dispersion behavior of the f-band, but it is rather limited to a small region around $\tilde{\Gamma}$. In analogy, the spectra for $LuRh_2Si_2$ shows a similar double peak structure between two dispersing Rh-bands, although the bands are slightly more separated and disperse oppositely more clearly.[28] Furthermore, as we change the energy, the intensity at E_F remains almost unchanged (not shown here), characteristic for a band without dispersion in the k_z-direction. Although the LDA+U+SOC calculation suggests that the anisotropic Coulomb interaction has a substantial influence on the $4f$-multilevel resulting in a clustering of $4f$ bands, we only observe two bulk bands centered at -1.3 eV and at -0.045 eV. Hence, in the future, we will neglect, for reasons of simplicity, the CEF effects and assume sharp and well defined 4f-excitations at energies ϵ_f and $\Delta\epsilon_f$, respectively.

Panels (C) and (D) of Fig. 7 show a photoemission spectrum $A(\overrightarrow{k},\omega)$ along the yellow line in Fig. 8. The top-left panel shows the raw data, the bottom left is the corresponding EDC analysis. The red circles are obtained by fitting a single peak and a constant background to the EDC curves and the red line is the Fermi level. A steep band (band (P_2) in Fig. 6) with strong Rh-d character hybridizes with the flat Yb f-band. This induces an opening of a band gap of the order of 30-40 meV. We note that this gap is too small to incorporate f-spectral weight into the FS.

These spectroscopic data yield the characteristic band structure of Yb-based material exhibiting a Kondo resonance below E_F.[31, 32] Increasing the temperature far above the Kondo temperature T_K induces a strong temperature dependence on the peak position and height and finally removes the peak.[29] In $YbRh_2Si_2$, the peak at $\tilde{\Gamma}$ however is removed due to the thermal broadening of the Fermi edge. No other temperature dependence of the peak position could be detected within the experimental resolution. Moreover, moving from $\tilde{\Gamma}$ to $\tilde{X}$ in reciprocal lattice, the spectrum does not follow the predictions for a Kondo resonance.

C. The analysis according the single-impurity model

Hybridization of electronic f-bands with a conduction band leads to peaks in the photoemission spectrum far off the energy of the f-levels (ϵ_f) [30–32]. The double-peak structure near $\tilde{\Gamma}$ also needs clarification with respect to Kondo resonance vs. an additional band, i.e. the Rh $4d_{x^2-y^2}$ band. Hence, a more elaborate data analysis is required. We employ a second-order perturbative calculation based on the Anderson single-impurity model. As mentioned in the previous section, we observe in the photoemission spectrum that the bulk $4f$-multiplet splits into $4f_{7/2}$- and $4f_{5/2}$-excitations separated by 1.3 eV. The additional splitting due to an anisotropic Coulomb interaction is not observed. In the following, the simulation will be referred to as the Gunnarsson-Schönhammer (GS) scheme. [31] For the Yb-4f shell we use the Ansatz for the ground state

$$|\Phi_0^{(1)}\rangle = A\left[|0\rangle + \int a(E)|E\rangle dE\right] \tag{2}$$

where

$$\begin{aligned} |0\rangle &= \prod_{\nu=1}^{14} \Psi_\nu^\dagger \prod_{\epsilon<\epsilon_F} \Psi_{\epsilon\nu}^\dagger |core\rangle \\ |E\rangle &= \frac{1}{\sqrt{N_f}} \sum_{\nu\prime=1}^{N_f} \Psi_{\nu\prime}\Psi_{E\nu\prime}^\dagger |0\rangle \end{aligned} \tag{3}$$

are the $4f^{14}$ and the $4f^{13}$ ions, respectively, and $\Psi_{E\nu\prime}^\dagger$ creates an electron in an unoccupied state. N_f is the degeneracy of states. Considering the large degeneracy, we calculated the energy-difference upon hybridization between the $4f^{14}$ ion and the hybridized state ΔE in first order, and obtained the same result as GS obtained for Ce-materials. The photoemission process T of relevance reduces the $4f$-shell by one electron, i.e.

$$T|\Phi_0^{(1)}\rangle = \sum_\nu \omega_\nu \Psi_{\tilde{E}\nu}^\dagger \Psi_\nu |\Phi_0^{(1)}\rangle \tag{4}$$

Contrary to previous postulations, there is no need for a mixed valency to observe the two sharp peaks at E_F

and -1.3 eV. In a hole language, this process adds a hole to the existing hole configuration. Following the reasoning of GS we obtained the result for the PE on Yb-ions corresponding to the inverse photoemission in cerium. Suggested by the photoemission result, we assumed $U = \infty$ and studied the $4f^{13}$ peak in detail. GS calculations were reported in many articles before. Our innovation is the inclusion and agreement of sophisticated band structure calculations. Considering the simplistic nearly-free electron approach from the previous section, we have parabola (P_1) ranging from -6 eV to 0 eV which is then continued above E_F in a second band with similar characteristics up to $\sim$ 6 eV. Hence, we can safely assume a half-filled semielliptical form for the hybridization of these bands with the $4f$-bands, ranging from -6 eV to 6 eV. For the band P_2 we use a nearly half-filled semielliptical form from -1.8 to 2.4 eV. The hybridization strength V is related to the splitting Δ by $\Delta = 2V^2/B$. The solution for the spectrum is equivalent to the solution for the BIS spectrum in cerium material, replacing the electrons by holes and inserting the form for the valence bands obtained from the band structure calculations. The 8-fold degenerate level is located at ϵ_f = -5 eV, the 6-fold at -6.3 eV. Now we adjust the hybridization strength V, respectively Δ in order to reproduce the spectrum.

The spectrum (open symbols) is obtained by integrating the angle-resolved photoemission data between 0° and 20° at 21.2 eV and subtracting the contribution from the Rh-4d band using a Doniach-Sunjic lineshape. [34] Furthermore, we subtracted the intensity from the $4f_{5/2}$ surface state centered at 2 eV using a Lorentzian and a uniform background as in Ref. [32]. The subtraction is rather tedious and a perfect agreement with the calculation cannot be expected. The features of interest are two strong intensity regions, one centered at -1.35 eV and one close to E_F. The feature at higher binding energy is slightly asymmetric, and some additional intensity around -1.1 eV could not be removed properly. The intensity maximum in $\rho_\nu(\epsilon)$ in the vicinity of E_F originates from the $4f_{7/2}$ hole final state and is about 25% higher than the $4f_{5/2}$ peak. The emission from the $4f_{7/2}$ surface state at 680 meV is approximated by a Lorentzian with line width $\sim$ 230 meV (see black dashed line). The best result is shown as a red solid line in the lower left panel of Fig. 7. The energy difference between the $4f^{14}$ and the hybridized state close to the $4f^{13}$-configuration is $\Delta E \sim$ -4.9 eV. From the simulation we can extract in first-order two hybridization strengths and 2 splittings separately. The gap for the interaction with parabola (P_1) yields Δ_1 $\sim$ 91 meV in excellent agreement with panel (A) of Fig. 7. The interaction with parabola (P_2) yields $\Delta_2 \sim$ 45 meV. This is the gap observed in the right panels of Fig. 7. The simulation yields a hole concentration of 0.98 in the $4f^{14}$ shell. The valence is hence +2.98, i.e. close to +3. The asymmetry of the peak at 50 meV can be explained by the arguments of Doniach and Sunjic. [34]

Haldane and Jefferson showed that using the "poor-man's scaling" technique, a single dimensionless energy

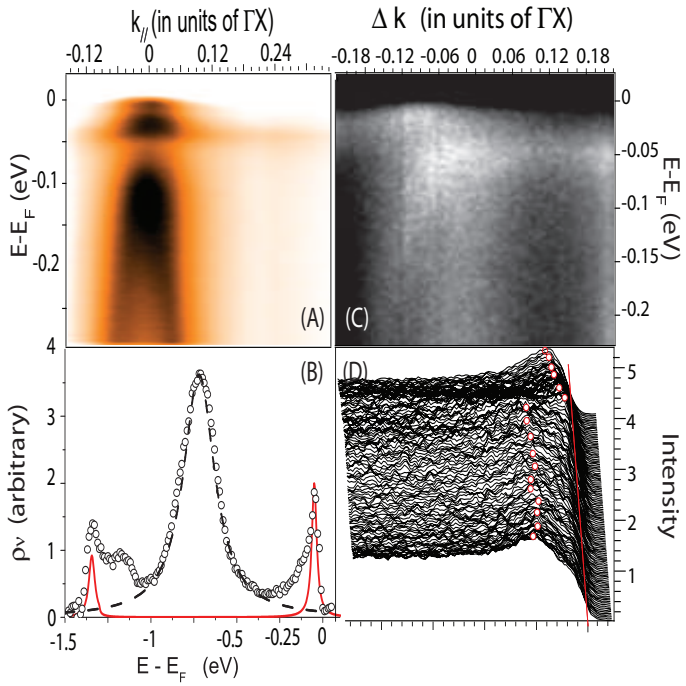

FIG. 7: (Color online) Panel (A): experimental PE spectrum for small energies in the vicinity of $\bar{\Gamma}$. Panel (B): The empty spectrum represent the spectrum solely due to the 4f final states obtained as explained in the text. The solid red line is a calculation according the GS-scheme explained in the text. The long-dashed line is a Lorentzian to the surface peak. The right panels show the hybridization of the f-band with the band (c). Panels (C) and (D) show the spectrum where band (c) and (1) hybridize and form a large FS. The zero denotes the wave vector $k_{||} = 0.385{\cdot}\Gamma X{\cdot}(0.985,0.174)$ and we measure along the yellow line in Fig. 8.

scale is needed,[41] which for $YbRh_2Si_2$ is

$$\epsilon_f^* \equiv \frac{\epsilon_f}{N_f \Delta} \approx -6.0eV \quad . \tag{5}$$

A very important temperature scale in a material with unfilled f-shells is given by the Kondo temperature T_K. We calculated the Kondo energy self-consistently using the expression in the GS-scheme

$$T_K \equiv \delta/k_B = \left(\epsilon_f + \frac{2}{\pi B}\int_{-B_{bot}}^{0} \frac{N_{f2}|V(\epsilon)|^2}{\epsilon - \delta}\right)/k_B \tag{6}$$

$$\approx (23 \pm 3)K \quad , \tag{7}$$

where k_B is the Boltzmann constant. This Kondo temperature is in excellent agreement with the results from macroscopic experiments which yielded $T_K \approx 24$ K [7, 8], considering the fact we used a simple second-order perturbative analysis of the experimental data.

Employing the dynamical theory of the degenerate Anderson model derived at zero temperature by Kuramoto and Müller-Hartmann [37], or in a more approx-

imate form by Newns and Hewson [38] yields the zero-temperature susceptibility

$$\chi_0(T=0K) = \frac{1}{3}\frac{j_1(j_1+1)}{2j_1+1} * g^2\mu_B^2\mu_0 N_A \frac{\pi}{\Delta E}\frac{n_f^2}{1-n_f} \quad (8)$$

$$\approx 1.4\cdot 10^{-5}\frac{mole}{m^3} \quad , \quad (9)$$

comparable to the result of $\sim 1.1{\cdot}10^{-5}$mole/m^3. Thus the Kondo coupling leaves a small moment which orders below 70 mK.[7] Additionally, we calculate the magnetic relaxation rate of the 4f electrons

$$\Gamma_M = \chi_0\left[lim_{\omega\to 0} Im\chi(\omega)/\omega\right]^{-1} = \frac{|N_f e_f^*|}{\pi n_f} \approx 10s^{-1} \quad . \quad (10)$$

This value is in again in very good agreement with the previously obtained results from ESR/NMR experiments on $YbRh_2Si_2$ at temperatures above 10 K, [11, 39] or for various other Yb-based materials, such as $YbCu_2$, $YbAl_2$ [40] in the regime where no field-dependence is observed.

We note a remarkable agreement of the parameters obtained using the GS simulation with those from macroscopic experiments. Hence, we confirm that SIAM is a simple but rather accurate tool for a quantification of the photoemission spectra in Yb-based materials [32, 35, 36] as we are limited to temperatures above the critical behavior. We notice that without the detailed knowledge of the band structure, finding a reasonable agreement between the SIAM calculations and the observed PE spectrum was nearly impossible. A description according the periodic Anderson model (PAM) using an angle-dependent matrix $V(\vec{k}, \vec{k}\,')$ was recently very successful in explaining a photoemission spectrum in $YbIr_2Si_2$.[27] The major complications in describing the macroscopic experiments such as resistivity and specific heat in $YbRh_2Si_2$ at low temperatures however raises a severe doubt on obtaining more information by description the spectrum using the PAM. In the same line of thinking, we have been checking for a temperature dependence of the two peaks in $A(\vec{k},\omega)$ near E_F and found no resemblance to a hump feature within the Kondo theory. The GS analysis suggests that the band structure is in good agreement with the experimental data, even though at first sight it seems anything but alike. The Kondo coupling shifts the spectral weight of the $4f_{7/2}$ quasiparticles close to E_F. The second peak at $\tilde{\Gamma}$ in the top panel of Fig. 7 arises indeed from the photoholes belonging to emissions out of the Rh-4$d_{x^2-y^2}$ band which is a stable component of this and other band structure calculations performed in this group.

We address the recent claim of $YbRh_2Si_2$ being a mixed valent. If a d-band overlaps the f-configuration and the Fermi energy overlaps the f configurational levels to within the hybridization energy, we have a mixed valence compound, i.e. the Yb ions occur either as Yb^{3+} with electronic $4f^{13}$ configuration or Yb^{2+} with $4f^{14}$ configuration. The panels (C) and (D) in Fig. 7 however display that the hybridization energy is smaller than the distance to the Fermi level, i.e. 50 meV, and hence no mixed valency can occur.

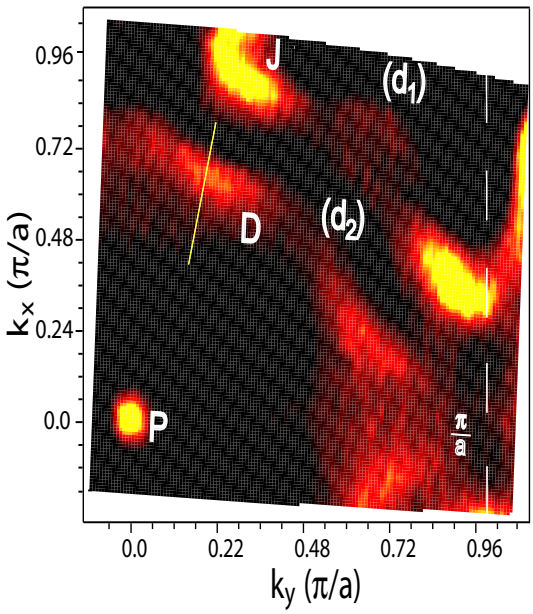

FIG. 8: (Color online) FS cut for $YbRh_2Si_2$. P denotes the Rh-4d_{xy} FS, D is the FS sheet centered around the upper zone face midpoint Z and J is a cut through the jungle gym FS consisting of two light holes sheet originating from the bands (d_1) and (d_2). The dashed line indicates $\frac{\pi}{a}$, where a is the length of the lattice basis. Units are given in $\frac{\pi}{a}$.

D. Fermi Surface at 21.2 eV

Fig. 8 shows a cut through the FS of $YbRh_2Si_2$ obtained at a photon energy of 21.2 eV. We integrated the intensity over an energy window of 2 meV at E_F. This integration window is extremely narrow urged by the shift of the spectral intensity of the $4f_{7/2}$ excitations by the Kondo interaction. In accordance with the FS from the LDA+U+SOC calculation, the FS splits into three different sheets. At $\tilde{\Gamma}$, there is a small pocket-like area P with a high intensity, which we interpreted as the Rh-4$d_{x^2-y^2}$ FS sheet. At the boundary of the BZ a very distinct FS sheet L of the form of a butterfly shows a strong intensity. As indicated by the cut along $\tilde{\Gamma}\tilde{X}$ in Fig. 6, two distinct sheets, labelled (d_1) and (d_2), respectively, form this electronic FS. An EDC analysis reveals that these excitations have a relatively light effective mass of m_{eff} $\approx$ 1.2 m_e. The intensity pattern labelled D shows a cut through the FS displaying Rh-4d and Yb-5d character.

Hence, the photoemission experiment shows that the FS obtained in the LDA+U+SOC calculation is at least

qualitatively, and probably even quantitatively, correct.

V. CONCLUSIONS

In this article we presented the results of an electronic band structure calculations in a relativistic framework including correlation corrections. Characteristic of the electronic structure is the $4f^{13}$ ground state as observed in the experiments with the $m = 0$ state unoccupied at 1.4 eV above E_F. A small FS cylinder of $4d_{x^2-y^2}$-symmetry is centered at Γ, a fluted donut $\mathcal{D}$ surface situated around the upper zone face midpoint Z and a multiply-connected jungle gym $\mathcal{J}$ surface. In the single particle picture the $4f$-multiplet splits into $4f$ complexes below -3.4 eV. The angle-resolved photoemission spectrum $A(\overrightarrow{k},\omega)$ manifests intensities originating from $4f^{13}_{7/2}$ and $4f^{13}_{5/2}$ states separated by 1.3 eV, the spin-orbit splitting obtained from the calculation. An analysis of the 4f-spectrum $\rho_\nu(\epsilon)$ according the degenerate Anderson impurity model using the parameters obtained from the band structure calculations explains the shift of the center of the $4f_{7/2}$ spectral weight to 45 meV below E_F. The estimated electronic gaps reproduce quantitatively the observed ones and indicate that the spectral weight of the f-bands are not taking part in actively forming the FS. Hence, $YbRh_2Si_2$ is not mixed-valent. The Kondo temperature $T_K \sim 23$ K, the valency $\sim +2.98$, the zero-temperature magnetic susceptibility $\chi_0 \sim 1.45{\cdot}10^{-5}$ mole/m^3 and the nuclear magnetic relaxation rate $\Gamma \sim 10.4$ s^{-1} are in excellent agreement with the results from macroscopic experiments. We also concluded that the tiny Rh-$4d_{x^2-y^2}$ crosses the Fermi level in accord with our band structure calculations. A FS map taken at 21.2 eV shows three sheets made of the Rh $4d_{x^2-y^2}$ cylinder near $\tilde{\Gamma}$, a sheet with high intensity embracing the X-point of the BZ and a large surface centered at the Z-point of the BZ.

The GS simulation indicates that a significant spectral weight is close to the Fermi level. We propose that the resistivity at low temperatures is dominated by the conduction of the electrons and holes in an ordinary way. The main scattering is due of spin-fluctuations having a continuum of low excitation energies as no indication for a preferred mode is seen in the spectrum for the light holes (l_1) and (l_2) within experimental resolution. This scattering mechanism displays a resistivity depending linearly on the temperature.

Previous ESR and especially the Hall Effect experiments rejected the theory of a SDW instability for the QCP in $YbRh_2Si_2$. Despite having these strong Si-bonds, which induce an easy-cleavage plane, and the observation of relatively sharp electronic bands, the electronic structure has to be considered highly three-dimensional, as can be seen from the results of the electronic band-structure calculation and a strong energy-dependence in $A(\overrightarrow{k},\omega)$. I.e. no net reduction in dimensionality is observed. The $4f$-bands are not participating in actively forming the FS. These observations severely conflict with the SDW theory. The analysis according the GS-scheme clearly proves that we are in the strong coupling limit. In this coupling regime, according to Senthil et al.,[17] the Fermi liquid phase of a material in the vicinity of the crossover from the RKKY-dominated to the Kondo-regime, form a "cold" and a "hot" FS sheet. The latter consists of the heavy quasiparticles and is considered to be large. The FS centered at $\tilde{\Gamma}$ is a small electronic pocket and hence can be disregarded. Accordingly, the portion $\mathcal{D}$ is the prime candidate for the "cold" FS. The FS sheet J would be the "hot" FS which is supposed to transform into a spin fluid with a FS of neutral spinons.[17] This experimental study clearly favors a three-dimensional approach to the theory of the quantum criticality in $YbRh_2Si_2$. It is at present not clear to the authors how the obvious electronic three-dimensionality can be reconciled with (quasi-)two-dimensional quantum critical fluctuations.

VI. ACKNOWLEDGEMENT

This work has benefited from partial financial support of the Schweizerische Nationalfonds zur Förderung der wissenschaftlichen Forschung, the US-DOE grant DE-FG03-01ER45876 and the grant NSF-DMR 0433560. W.E.P. acknowledges support and stimulating atmosphere of the Department of Energy's Stewardship Science Academic Alliances Program, and the hospitality of the Alexander von Humboldt Foundation during the latter stages of this work.

[1] G.R. Stewart, Rev. Mod. Phys. **73**, 797 (2001).
[2] B. Bogenberger and H. v. Lohneysen, Phys. Rev. Lett. **74**, 1016 (1995).
[3] F.M. Grosche, S.R. Julian, N.D. Mathur, and G.G. Lonzarich, Physica B, **223-224**, 50 (1996).
[4] I.R. Walker, F.M. Grosche, D.M. Freye, and G.G. Lonzarich, Physica C, **282-287**, 303 (1997).
[5] P. Estrella, A. de Visser, F.R. de Boer, G.J. Nieuwenhuys, L.C.J. Pereira and M. Almeida, Physica B **259-261** 409 (1999).
[6] M.A. Ruderman and C. Kittel, Phys. Rev. **96**, 99 (1954).
[7] O. Trovarelli, C. Geibel, S. Mederle, C. Langhammer, F.M. Grosche, P. Gegenwart, M. Lang, G. Sparn, and F. Steglich, Phys. Rev. Lett. **85**, 626 (2000).
[8] P. Gegenwart, J. Custers, C. Geibel, K. Neumaier, T. Tayama, K. Tenya, O. Trovarelli, and F. Steglich, Phys. Rev. Lett. **89**, 056402 (2002).
[9] O. Trovarelli, J. Custers, P. Gegenwart, C. Geibel, P. Hinze, S. Mederle, G. Sparn and F. Steglich, Physica B **312-313**, 401 (2002).

[10] J. Custers, P. Gegenwart, H. Wilhelm, K. Neumaler, Y. Tokiwa, O. Trovarelli, C. Geibel, F. Steglich, C. P*é*pin and P. Coleman, Nature **424**, 524 (2003).

[11] K. Ishida, D.E. MacLaughlin, O.O. Bernal, R.H. Heffner, G.J. Nieuwenhuys, O. Trovarelli, C. Geibel and F. Steglich Physica B **326**, 403 (2003).

[12] K. Ishida, K. Okamoto, Y. Kawasaki, Y. Kitaoka, O. Trovarelli, C. Geibel, and F. Steglich Phys. Rev. Lett. **89**, 107202 (2002).

[13] S. Paschen, T. Luhmann, S. Wirth, P. Gegenwart, O. Trovarelli, C. Geibel, F. Steglich, P. Coleman, Q. Si, Nature **432**, 881 (2004).

[14] M.R. Norman, Phys. Rev. B **71**, 220405 (2005).

[15] J.A. Hertz, Phys. Rev. B **14**, 1165 (1976).

[16] A.J. Millis, Phys. Rev. B **48**, 7183 (1993).

[17] T. Senthil, S. Sachdev and M. Vojta, Phys. Rev. Lett. **90**, 216403 (2003).

[18] T. Senthil, M. Vojta and S. Sachdev, Phys. Rev. B **69**, 035111 (2004).

[19] C. Pépin, Phys. Rev. Lett. **94**, 066402 (2005).

[20] Q. Si, S. Rabello, K. Ingersent and J.L. Smith, Nature **413**, 804 (2001).

[21] Q. Si, S. Rabello, K. Ingersent, J.L. Smith, Phys. Rev. B **68**, 115103 (2003).

[22] S. Hüfner, *Photoelectron Spectroscopy* (Springer Verlag, Berlin, 1995).

[23] P.W. Anderson, Phys. Rev. **124**, 41 (1961).

[24] K. Schwarz, P. Blaha and G. K. H. Madsen, Comput. Phys. Commun. **147**. 71 (2002).

[25] J. P. Perdew, K. Burke, and M. Ernzerhof, Phys. Rev. Lett. **77**, 3865 (1996).

[26] M.D. Johannes and W.E. Pickett, Phys. Rev. B **72**, 195116 (2005).

[27] S. Danzenbächer, Y. Kucherenko, C. Laubschat, D.V. Vyalikh, Z. Hossain, C. Geibel, N. Mannella, X.J. Zhou, W. Yang, Z.-X. Shen and S.L. Molodstov, Phys. Rev. Lett. **96**, 106402 (2006).

[28] We intend to publish a complete discussion on the band structure and the Fermi surface of $YbRh_2Si_2$, including results for $LuRh_2Si_2$ and $LaRh_2Si_2$.

[29] L.H. Tjeng, S.-J. Oh, E.-J. Cho, H.-J. Lin, C.T. Chen, G.-H. Gweon, J.-H. Park, J.W. Allen, T. Suzuki, M.S. Makivić and D.L. Cox, Phys. Rev. Lett. **71**, 1419 (1993).

[30] J.W. Allen, S.-J. Oh, I. Lindau, J.M. Lawrence, L.I. Johansson and S.B. Hagström, Phys. Rev. Lett. **81**, 1100 (1981); J.W. Allen, G.H. Gweon, H.T. Schek, L.Z. Liu, L.H. Tjeng, J.H. Park, W.P. Wllis, C.T. Chen, O. Gunnarsson, O. Jepsen, O.K. Andersen, Y. Dalichaouch, J. Appl. Phys. **87**, 6088 (2000).

[31] O. Gunnarsson and K. Schönhammer, Phys. Rev. B **28**, 4315 (1983).

[32] F. Patthey, J.-M. Imer, W.-D. Schneider, H. Beck, Y. Baer and B. Delley, Phys. Rev. B **42**, 8864 (1990).

[33] N.E. Bickers, D.L. Cox and J.W. Wilkins, Phys. Rev. Lett. **54**, 230 (1985).

[34] S. Doniach and M. Sunjic: J. Phys. C **3**, 285 (1970).

[35] F. Patthey, J.-M. Imer, W.-D. Schneider, Y. Baer, B. Delley, and F. Hulliger, Phys. Rev. B **36**, 7697 (1987).

[36] S.-J. Oh, S. Suga, A. Kakizaki, M. Taniguchi, T. Ishii, J.-S. Kang, J.W. Allen, O. Gunnarsson, N.E. Christensen, A. Fujimori, T. Suzuki, T. Kasuya, T. Miyahara, H. Kato, K. Schönhammer, M.S. Torikachvili, M.B. Maple, Phys. Rev. B **37**, 2861 (1988).

[37] Y. Kuramoto and E. Müller-Hartmann, J. Magn. Mag. Materials, **52**, 122 (1985).

[38] D.M. Newns and A.C. Hewson, J. Phys. F **10**, 2429 (1980).

[39] J. Sichelschmidt, V.A. Ivanshin, J. Ferstl, C. Geibel and F. Steglich, Phys. Rev. Lett. **91**, 156401 (2003).

[40] A. Fujimori, T. Shimizu and H. Yasuoka, Phys. Rev. B **35**, 8945 (1987).

[41] F.D.M. Haldane, Phys. Rev. Lett. **40**, 416 (1978), or J.H. Jefferson, J. Phys. C **10**, 3589 (1997).